

1

Elastic Registration and Shape Analysis of Functional Objects

Zhengwu Zhang, Qian Xie, and Anuj Srivastava

Florida State University

1.1 Introduction

Professor Kanti Mardia and his colleagues have led the advancement of ideas and tools in the field of statistical shape analysis of objects for over two decades. This progress has been triggered by a confluence of tools from geometry, statistics, computing, and imaging, and has continued in several interesting directions. One area that has seen an increasing focus is the joint solution to registration and shape comparison problems. Traditionally, shape analysis has been performed on finite point sets that have been labeled or registered, i.e. one is given a correspondence between points across the sets (Dryden and Mardia 1998; Mardia and Dryden 1989). However, in many real applications, especially those involving image data, this correspondence may not be available. Thus, one has to solve for the registration problem as part of shape analysis. While some early efforts took a sequential approach, where one registers the objects first and then uses this registration in subsequent shape analysis, it quickly became clear that a more comprehensive, joint solution is needed. Thus, the simultaneous registration and shape analysis of objects became an important goal in the shape analysis. In this paper we summarize advances in *elastic shape analysis*, a class of Riemannian solutions that provide a metric-based framework for registration of points while using the same metric for shape comparisons.

The objects of interest in shape analysis can vary according to applications. While shapes of planar, closed contours are of prime interest in image analysis and computer vision, where objects' boundaries help us classify objects and their motions, there is also interest in other types of objects. Some problems require analyzing shapes of curves in more than two dimensions. An example is protein structure analysis where one studies shapes of protein backbones (Liu et al. 2010, 2011), as curves in \mathbb{R}^3 . Another object of interest is the shape of surfaces as embeddings of spheres or discs in \mathbb{R}^3 (Kuttek et al. 2012a). This is useful, for instance, in medical imaging where one studies shapes of anatomical structures for the

purpose of diagnosing medical conditions. Shape analysis of surfaces that form boundaries of 3D objects has also found interest in computer graphics, 3D printing, and visualization. There are also problem areas that do not directly involve shapes but where the ideas and methods derived from shape considerations can contribute significantly. An example is the problem of alignment of real-valued functions, the so-called phase-amplitude separation in functional data analysis in Tucker et al. (2012, 2013), that has benefited from metrics and procedures developed initially for shape analysis of curves. Such alignment problems also arise in image registration where a *metric-based* approach offers significant advantages in Xie et al. (2012). The extensions of shape analysis of Euclidean curves have also led to formal studies for comparisons and modeling of trajectories on Riemannian manifolds in Su et al. (2014).

1.1.1 From Discrete to Continues and Elastic

As mentioned earlier, a large majority of past statistical analyses of shapes use discrete, point-set representations, while the more recent trend is to study continuous objects. Since continuous objects, such as parameterized curves and surfaces, are represented by coordinate functions, and functional spaces are typically infinite-dimensional, this change introduces an additional complexity of infinite-dimensionality. So, the question arises: Are we making the problem unnecessarily complicated by using functional representations? Let us study the options more carefully. Say we are given two sets, each set contains a finite number of unregistered points, and our goal is to register them and to compare their shapes. Now the problem of registration is a combinatorial one and adds considerable computational complexity to the solution. On the other hand, let us assume the original objects are parameterized curves: $t \mapsto (f_1(t), f_2(t))$, for $t \in D$ where D is an appropriate domain. The interesting part in this approach is the following. For each t , the pair of points, $f_1(t)$ and $f_2(t)$ are considered registered. In order to change the registration, one simply has to re-parameterize one of the objects. In other words, find a re-parameterization γ of f_2 such that $f_1(t)$ is now registered to $f_2(\gamma(t))$. Thus, we can find optimal registration (or alignment) of curves by optimizing over the variable γ under a proper objective function. If this objective function is a metric that is invariant of all shape-preserving transformations, then we simultaneously achieve a joint solution for registration and shape comparison. Thus, parameterization controls registration between curves and an optimal registration can be found using algorithms with complexity much smaller than those encountered in combinatorial solutions. Similar arguments can be made for higher-dimensional parameterized objects, such as surfaces and images, as well. The optimization over parameterization variability in shape analysis of objects, under a metric with proper invariance properties, leads to a framework called *elastic shape analysis*. In this chapter we will summarize the progress in elastic shape analysis of different types of continuous objects, and will point out some fundamental issues – theoretical and computational – in these areas.

1.1.2 General Elastic Framework

Here onwards we will focus exclusively on parameterized objects – functions, curves, surfaces, images, trajectories – and use parameterizations to control registrations.

For different types of objects, the choice of mathematical representations and domains will be different. In case of functional data analysis (FDA) and shape analysis of curves,

the domain of interest is $D = [0, 1]$; for analyzing shapes of surfaces it is $D = \mathbb{S}^2$ and for performing registration of 2D images, it is $D = [0, 1]^2$. The re-parameterization is chosen to be a direction- and boundary-preserving diffeomorphism from D to itself, and Γ is the set of all such diffeomorphisms. For instance, in case of FDA, Γ is the set of all positive diffeomorphisms such that $\gamma(0) = 0$ and $\gamma(1) = 1$. Similarly, for shape analysis of surfaces Γ includes all orientation-preserving diffeomorphisms of \mathbb{S}^2 to itself. An interesting property of Γ is that it forms a group action under composition, with the identity element given by the function $\gamma_{id}(t) = t$. Therefore, for any two γ_1, γ_2 , the composition $\gamma_1 \circ \gamma_2$ is also a valid re-parameterization, and so is the inverse γ^{-1} for any γ .

The next issue is to decide the objective function so that optimal re-parameterization can be found in a variational framework. A seemingly natural idea of performing alignment using the criterion $\inf_{\gamma} \|f_1 - f_2 \circ \gamma\|$, where $\|\cdot\|$ denotes the \mathbb{L}^2 norm, turns out to be problematic. The main issue is that it allows degeneracy, that is, one can reduce this cost arbitrarily close to zero even when the two functions may be quite different. This is commonly referred to as the *pinching problem* in Ramsay and Silverman (2005). Pinching implies that a severely distorted γ is used to eliminate (or minimize) those parts of f_2 that do not match with f_1 ; this can be done even when f_2 is mostly different from f_1 . Another way to state the problem is that one can easily manipulate $\|f \circ \gamma\|$ into a broad range of values, by choosing an appropriate γ . Of course, one can avoid the pinching problem by imposing a roughness penalty on γ , thus avoiding a severe distortion of γ s, but that leads to other issues including asymmetry. A related problem from the registration perspective is that: $\|f_1 - f_2\| \neq \|f_1 \circ \gamma - f_2 \circ \gamma\|$ in general. Why is this problematic? Observe that if we warp two functions by the same γ : earlier $f_1(t)$ matches with $f_2(t)$, and now $f_1(\gamma(t))$ matches with $f_2(\gamma(t))$. Each point-wise registration remains unchanged but their \mathbb{L}^2 norm changes. Hence, the \mathbb{L}^2 norm is not a proper objective function to help solve the registration problem.

The solution comes from deriving an elastic-metric based objective function that is better suited for registration and shape comparison. While the discussion of the underlying elastic Riemannian metric is complicated, we directly move on to a simplification which is based on certain square-root transforms of data objects. Denoted by q , these objects take different mathematical forms in different contexts, as explained in later sections. The important mathematical property of these representations is that $\|q_1 - q_2\| = \|(q_1, \gamma) - (q_2, \gamma)\|$, for all γ , where q_i s represent the objects f_i s and (q_i, γ) represents the re-parameterized object $(f_i \circ \gamma)$. This property allows us to define a solution for all important problems:

$$\inf_{\gamma} \|q_1 - (q_2, \gamma)\| = \inf_{\gamma} \|(q_1, \gamma) - q_2\| \quad (1.1)$$

Not only does the optimal γ help register the object f_2 to f_1 , but also the infimum value of the objective function is a proper metric for shape comparison of the two objects. (In case of shape analysis of curves and surfaces one needs to perform an additional rotation alignment for shape comparisons.) This metric enables statistical analysis of shapes. One can compute mean shapes and the dominant modes of variations in a shape sample, develop statistical models for capturing observed shape variability, and use these models in performing hypothesis tests. While we focus on static shapes in this chapter, these ideas can also be naturally extended to dynamic shapes.

In the next few sections we demonstrate applications of this elastic framework in the contexts of functional data analysis, shape analysis of parametrized curves, shape analysis of surfaces and 2D image registration.

1.2 Registration in FDA: Phase-Amplitude Separation

Recent years have seen an increasing involvement of functional data in statistical analyses (Kneip and Ramsay 2008; Ramsay and Li 1998; Ramsay and Silverman 2005; Tang and Muller 2008). The variables of interest here are functions on certain intervals, and one is interested in using these variables in a variety of problems, including modeling, prediction, and regression. Examples of functional data include growth curves, mass spectrometry data, bio-signals, human activity data, and so on. These observations are typically treated as square-integrable functions, with the resulting set of functions forming an infinite-dimensional Hilbert space. The standard \mathbb{L}^2 inner-product, $\langle f_1, f_2 \rangle = \int f_1(t)f_2(t)dt$, provides the Hilbert structure for comparing and analyzing functions. For example, one can perform function principal component analysis (FPCA) of a given set $\{f_i\}$ using this Hilbert structure. Similarly, a variety of ideas, such as the functional linear regressions, partial least squares, etc, have been proposed for working with functional data.

A difficulty arises when the observed functions exhibit variability in their arguments. In other words, instead of observing a function $f(t)$ on an interval, say $[0, 1]$, one observes a “time-warped” function $f(\gamma(t))$ where γ is a time-warping function. This extraneous effect, termed *phase variability*, has the potential to add artificial variance in the observed data and needs to be accounted for in statistical analysis. Let $\{f_i\}$ be a set of observations of a functional variable f . Then, for any time t , the observations $\{f_i(t)\}$ have some inherent variability. However, if we observe $\{f_i \circ \gamma_i\}$ instead, for random warpings γ_i s, then the resulting variability in $\{f_i(\gamma_i(t))\}$ has been enhanced due to random γ_i s. The problem of registration of functional data, also called *phase-amplitude separation*, is an important one (Srivastava et al. 2011b; Tucker et al. 2013). Given a set of functions $\{f_i\}$ on a common interval, say $[0, 1]$, the goal is to find a set of warping functions $\{\gamma_i\}$, such that $\{f_i \circ \gamma_i\}$ are aligned/registered. Let Γ denote the set of all warping functions (positive diffeomorphisms from $[0, 1]$ to itself).

We illustrate a solution to this problem based on a Riemannian metric that has origins in information geometry. This metric can be viewed as an extension of the classical Fisher-Rao metric, or rather its nonparametric version, from pdfs to more general class of functions as mentioned in Srivastava et al. (2011b). While the original form of this metric is quite complicated, a simplification results from a simple change of variable. For a function $f : [0, 1] \rightarrow \mathbb{R}$, define a new function called the *square-root slope function* (SRSF) according to:

$$q : [0, 1] \rightarrow \mathbb{R}, q(t) = \text{sign}\{\dot{f}(t)\} \sqrt{|\dot{f}(t)|} \quad .$$

If the original f is absolutely continuous, then the resulting q is square integrable. Srivastava et al. (2011b) has shown that the Fisher-Rao metric becomes the \mathbb{L}^2 metric under the change of variable $f \rightarrow q$. Let f_1, f_2 be two functions that need to be registered and let q_1, q_2 be their SRSFs. Then, the registration problem is solved by:

$$\inf_{\gamma \in \Gamma} \|q_1 - (q_2 \circ \gamma)\sqrt{\dot{\gamma}}\| = \inf_{\gamma \in \Gamma} \|q_2 - (q_1 \circ \gamma)\sqrt{\dot{\gamma}}\| \quad . \quad (1.2)$$

The optimization is performed using a numerical procedure called the *dynamic programming algorithm*. Fig. 1.1 shows an example of this alignment between two Gaussian density functions. After optimization, the two functions are nicely aligned, as shown in the middle panel, and the resulting optimal warping γ^* is shown in the right panel.

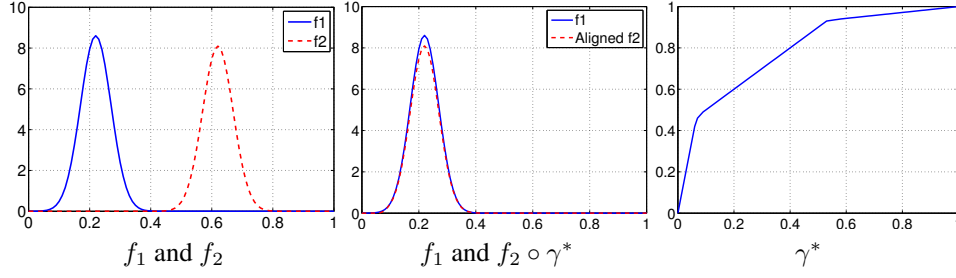


Figure 1.1 Alignment of two functions: align f_2 to f_1 . The middle panel shows the aligned result.

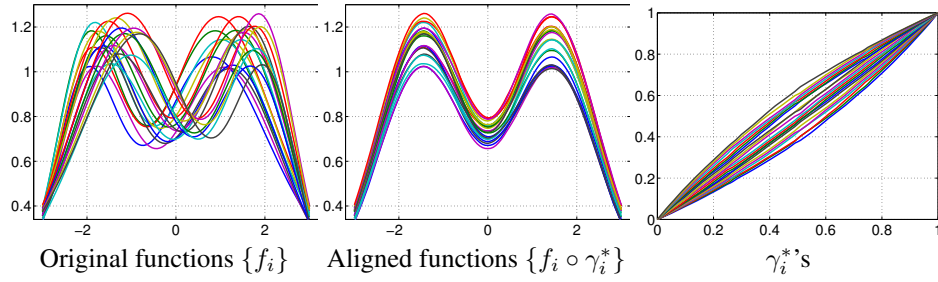


Figure 1.2 Multiple functions alignment. The leftmost panel shows a set of functions which have different height and peak locations. The middle panel shows the aligned result, and the right panel shows the optimal warping function γ_i^* 's.

In case we have multiple functions that need to be aligned, we can extend the previous pairwise alignment as follows. We use the fact that the quantity in Eqn. 1.2 is actually a proper metric in a certain quotient space, and use it to define a mean function. This mean function serves as a template for aligning other functions, i.e. each function is aligned to this mean function. In fact, the problem of multiple alignment and mean computation are formulated and solved jointly using an iterative procedure: initialize the mean function μ and iteratively solve for

$$\begin{aligned} \gamma_i &= \arg \inf_{\gamma \in \Gamma} \|\mu - (q_i \circ \gamma)\sqrt{\gamma}\|, i = 1, 2, \dots, n, \text{ and} \\ \mu &= \frac{1}{n} \sum_{i=1}^n (q_i \circ \gamma_i) \sqrt{\gamma_i} \quad . \end{aligned} \quad (1.3)$$

A synthetic example of multiple functions alignment is shown in Fig. 1.2. The leftmost panel shows a number of bimodal functions in which the heights and locations of peaks are different. The aligned functions are shown in the middle panel, and the optimal warping functions γ_i 's are shown in the right panel.

Next we show one example of the multiple functions alignment in a real dataset: the Berkeley growth dataset which contains 54 female and 39 male subjects. To better illustrate,

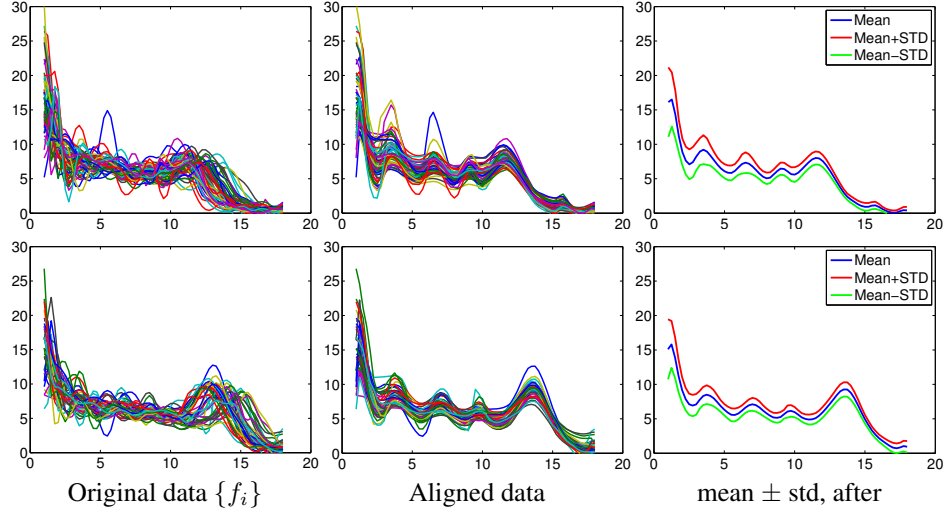


Figure 1.3 Analysis of growth data. Top row shows the growth data for 54 females, and the bottom row shows the growth data for 39 males.

we analyze the first derivatives of the growth curves. The results are shown in Fig. 1.3. Top row shows the alignment result for 54 female subjects and the bottom row shows the alignment result for 39 male subjects. The last column shows the mean \pm (cross sectional) standard deviation plot after the alignment. From the result, one can see that while the growth spurts for different individuals occur at slightly different times, there are some underlying patterns to be discovered.

1.3 Elastic Shape Analysis of Curves

The framework for function alignment can be easily extended to perform shape analysis of parameterized curves. Here the objects of interest are given by parameterized curves $f : [0, 1] \rightarrow \mathbb{R}^n$. (Note that in case of closed curves it is natural to use \mathbb{S}^1 as the parameterization domain, rather than an interval.) The \mathbb{L}^2 metric is given by $\langle f_1, f_2 \rangle = \int_0^1 \langle f_1(t), f_2(t) \rangle dt$ and the resulting norm $\|f_1 - f_2\| = \sqrt{\int_0^1 |f_1(t) - f_2(t)|^2 dt}$, where $|\cdot|$ denotes the vector norm. The mathematical representation of curves is in form of the *square-root velocity function* (SRVF) given by Srivastava et al. (2011a) and Kurtek et al. (2012b):

$$q : [0, 1] \rightarrow \mathbb{R}^n, q(t) = \frac{\dot{f}(t)}{\sqrt{|\dot{f}(t)|}} \quad .$$

The re-parameterization group here is the set of all positive diffeomorphisms of $[0, 1]$. If q is the SRVF of a curve f , then the SRVF of the re-parameterized curve $f \circ \gamma$ is given by $(q \circ \gamma)\sqrt{\dot{\gamma}}$; we will denote this by (q, γ) . Other simple representations of planar curves have been presented in Bauer et al. (2013).

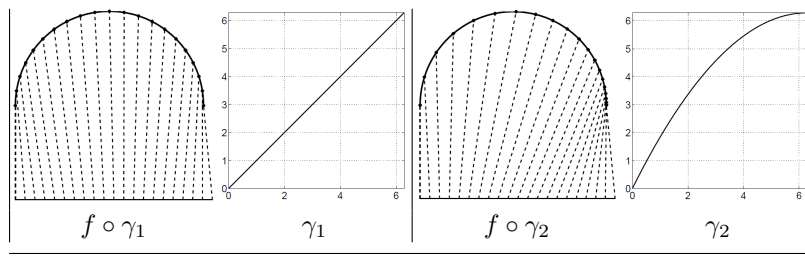


Figure 1.4 An illustration of re-parameterization curve in domain $D = [0, 2\pi]$.

From the perspective of shape analysis, a rigid motion (or translation), re-parameterization, rotation and scaling of a curve do not alter its shape. The translation has been removed by the SRVF representation automatically. An illustration of different parameterizations of a curve is shown in Fig. 1.4. The shape of f is exactly the same as the shape of $f \circ \gamma$, for any γ . The same holds for the rigid rotation of a curve. For any $O \in SO(n)$, the rotated curve $O f(t)$ has the same shape as the original curve. If we do not consider the scaling for the moment, this leads to formulation of equivalence classes, or orbits, of representations that all correspond to the same shape. Let $[f]$ denote all possible translations, rotations and re-parameterizations of a curve f . The corresponding set in SRVF representation is given by $[q] = \{O(q, \gamma) | O \in SO(n), \gamma \in \Gamma\}$. Each such class represents a shape uniquely and shapes are compared by computing a distance between the corresponding orbits.

As mentioned earlier, the SRVF representation satisfies the property that $\|q\| = \|(q, \gamma)\|$, and $\|q_1 - q_2\| = \|(q_1, \gamma) - (q_2, \gamma)\|$ for all $\gamma \in \Gamma$ and all q, q_1, q_2 . Using this property, the shape distance between any two shapes is given by:

$$d([q_1], [q_2]) = \inf_{\gamma \in \Gamma, O \in SO(n)} \|q_1 - O(q_2, \gamma)\| = \inf_{\gamma \in \Gamma, O \in SO(n)} \|O(q_1, \gamma) - q_2\| \quad (1.4)$$

This optimization emphasizes the joint nature of our analysis – on the one hand we optimally register points across two curves using re-parameterization and rotation, and on the other hand we obtain a metric for comparing shapes of the two curves. The optimization over $SO(n)$ and Γ is performed using coordinate relaxation – optimizing over one variable while fixing the other. The optimization over $SO(n)$ uses the Procrustes method while the optimization over Γ uses the dynamic programming algorithm (Srivastava et al. 2011a). In absence of any other constraints on the curves, a straight line between q_1 and the registered q_2 , i.e. $O^*(q_2, \gamma^*)$, with these quantities being the minimizers in the equation 1.4, forms the desired geodesic. However, if we rescale the curves to be of unit length or restrict ourselves to only the closed curves, then the underlying space becomes nonlinear and requires additional techniques for computing geodesics. We have developed a path-straightening algorithm for computing geodesics in the shape space of closed curves under the elastic metric, as described in Srivastava et al. (2011a). Fig. 1.5 shows some examples of geodesic paths between several pairs of closed curves taken from the MPEG7 dataset (Jeannin and Bober 1999). One can see that this joint framework deforms one shape to another in a natural way – the features are

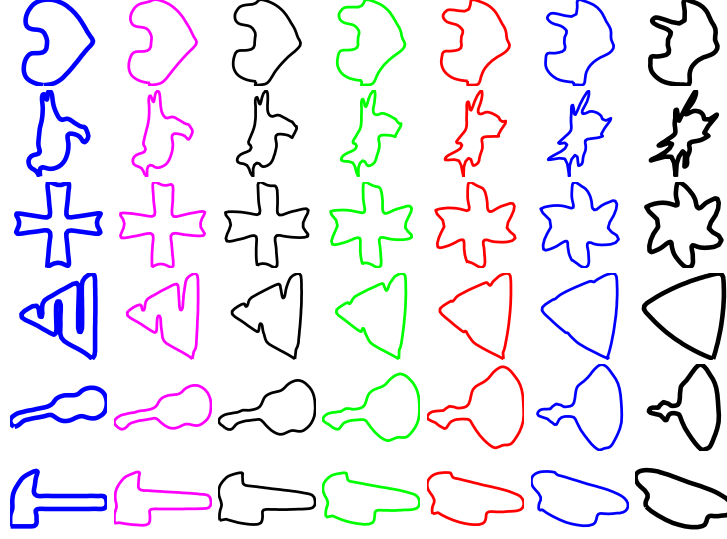


Figure 1.5 Each row shows an example of geodesic path between the starting and ending shapes under the elastic framework.

better preserved across shapes and deformations are smooth.

Mean Shape and Modes of Variations: This framework is amenable to the development of tools for statistical analysis of shapes. For example, given a set of observations of curves, we may want to calculate the sample mean and modes of variations. Furthermore, we are interested in capturing the variability associated with the shape samples using probability models. The notion of a sample mean on a nonlinear manifold is typically defined using the Karcher mean (Karcher 1977). Let f_1, f_2, \dots, f_n be the observed sample shapes and q_1, q_2, \dots, q_n be the corresponding SRVFs. The Karcher mean is defined as a quantity that satisfies: $[\mu] = \operatorname{argmin}_{[q]} \sum_{i=1}^n d([q], [q_i])^2$, where $d([q], [q_i])$ is calculated using Eqn. 1.4, and μ is the SRVF representation of the mean shape \bar{f} . The search for the optimal mean shape \bar{f} can be solved using an iterative gradient-based algorithm (Karcher 1977; Kurtek et al. 2012b; Srivastava et al. 2005). Fig. 1.6 shows some sample mean shapes calculated using this approach.

In addition to the Karcher mean, the Karcher covariance and modes of variation can be calculated to summarize the given sample shapes. Since the shape space is non-linear, we can use the tangent space at the mean shape μ , which is a standard vector space, to perform the statistical analysis. We first map each sample shape onto the tangent space using inverse exponential map: $v_i = \log_{\mu}(q_i)$, then we define the covariance matrix to be: $C = \frac{1}{n-1} \sum_{i=1}^n v_i v_i^t$. Using Principal Component Analysis (PCA) of C , we can get the modes of shape variation. If PC_k denotes the k -th principal direction, then the exponential map $\exp_{\mu}(t \text{PC}_k s_k)$ as a function of t shows the shape variation in PC_k principal direction with standard deviation s_k .

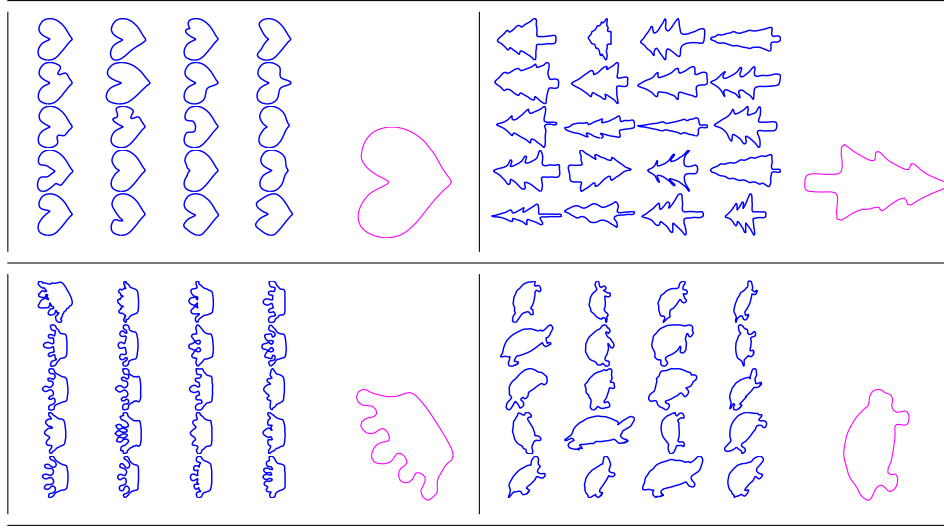


Figure 1.6 Mean shapes of four different classes of shapes. Each mean shape (shown in magenta color) is calculated from shapes on its left.

Fig. 1.7 shows the modes of variations for different classes of shapes in Fig. 1.6.

Statistical Shape Models: After obtaining the mean and covariance, the further step is to develop probability models to capture the distribution of given sample shapes. It is challenging to directly impose a probability density on the non-linear shape space. A common solution is to impose a distribution on a finite subspace of the tangent vector space. For example, one can restrict to principal subspace of the tangent space at mean μ . Then, we can impose a multivariate Gaussian distribution on the principal subspace with zero mean and covariance matrix obtained from the sample shapes. Fig. 1.8 shows the examples of random samples using means and covariance matrices estimated from shapes shown in Fig. 1.6.

While traditional shape analysis removes the transformations resulting from rigid motions and global scaling in shape considerations, in elastic shape analysis we additionally remove the effects of re-parameterizations. In some situations, however, there is a need for removing other groups such as the affine and projective groups. For a discussion on the resulting affine-elastic shape analysis of planar curves, we refer the reader to the paper Bryner et al. (2014). This paper also describes a framework for projective-invariant shape analysis of planar objects but using point-set representations rather than continuous curves, using the ideas first proposed in Kent and Mardia (2012).

1.4 Elastic Shape Analysis of Surfaces

The task of comparing shapes of 3D objects is of great interest in many important applications. For instance, the shapes of anatomical parts can contribute in medical diagnoses,

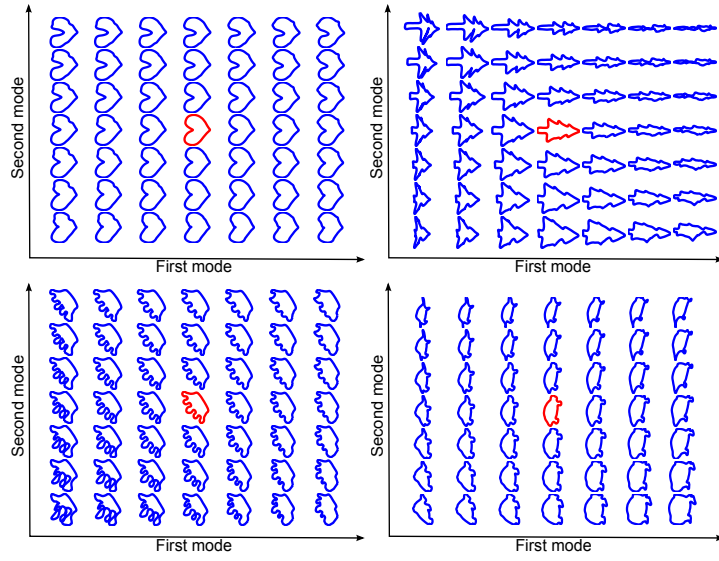


Figure 1.7 Modes of variations: for each class of shapes in mean shape examples (Fig. 1.6), we show the variation along the first and second principal modes. Shape in the center is the mean shape.

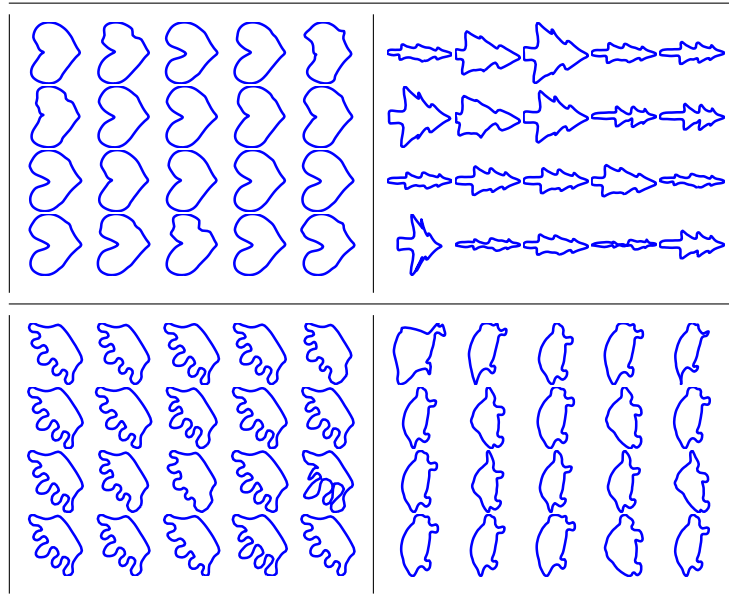


Figure 1.8 Random samples from the Gaussian shape distribution of different classes of shapes.

including monitoring the progression of diseases (Grenander and Miller 1998; Kurtek et al. 2011; Samir et al. 2014). The main challenge in such shape analysis comes from the fact that image data are often collected from different coordinate systems and data registration becomes a critical part of the analysis. In the following discussion, we will focus on surfaces that are embeddings of a unit sphere \mathbb{S}^2 in \mathbb{R}^3 . In other words, the surfaces of interest can be parameterized using the sphere according to a mapping $f : \mathbb{S}^2 \rightarrow \mathbb{R}^3$. For any $s \in \mathbb{S}^2$, the vector $f(s) \in \mathbb{R}^3$ denotes the Euclidean coordinates of that point on the surface. The domain of interest is $D = \mathbb{S}^2$, and the \mathbb{L}^2 metric is given by $\langle f_1, f_2 \rangle = \int_{\mathbb{S}^2} \langle f_1(s), f_2(s) \rangle m(ds)$, with $m(ds)$ denoting the Lebesgue measure on \mathbb{S}^2 , and the resulting norm is $\|f_1 - f_2\| = \int_{\mathbb{S}^2} |f_1(s) - f_2(s)|^2 m(ds)$. Let (u, v) denote the local coordinates of a point $s \in \mathbb{S}^2$. Then, the vectors $\frac{\partial f}{\partial u}(s)$ and $\frac{\partial f}{\partial v}(s)$ span the two-dimensional space tangent to the surface at point $f(s)$ and

$$n(s) = \frac{\partial f}{\partial u}(s) \times \frac{\partial f}{\partial v}(s)$$

is a vector normal to the surface at $f(s)$. Its magnitude $|n(s)| = \sqrt{\langle n(s), n(s) \rangle}$ denotes infinitesimal area of the current parameterization at that point and the ratio $n(s)/|n(s)|$ gives the unit normal vector. The mathematical representation of surfaces, suitable for elastic shape analysis, given by the *square-root normal field* (SRNF) defined as (Jermyn et al. 2012; Xie et al. 2013):

$$q : \mathbb{S}^2 \rightarrow \mathbb{R}^3, q(s) = \frac{n(s)}{\sqrt{|n(s)|}} \quad .$$

The re-parameterization group here is the set of all positive diffeomorphisms of \mathbb{S}^2 . If q is the SRNF of a surface f , then the SRNF of the re-parameterized surface $f \circ \gamma$ is given by $(q \circ \gamma)\sqrt{J_\gamma}$, where J_γ is the determinant of the Jacobian matrix of the mapping $\gamma : \mathbb{S}^2 \rightarrow \mathbb{S}^2$. We will denote this by (q, γ) . Similar to the identities presented for previous two cases, this representation also follows the isometry conditions: for all surfaces f , f_1 , and f_2 , and the corresponding SRNFs q , q_1 , and q_2 , and all $\gamma \in \Gamma$, we have: $\|q\| = \|(q, \gamma)\|$ and $\|q_1 - q_2\| = \|(q_1, \gamma) - (q_2, \gamma)\|$.

Once again, from the perspective of shape analysis, a re-parameterization and a rotation of a surface does not alter its shape. The shape of f is exactly same as the shape of $O(f \circ \gamma)$, for any $\gamma \in \Gamma$ and $O \in SO(3)$. This motivates the formulation of equivalence classes, or orbits, of representations that all correspond to the same shape. Let $[f]$ denote all possible rotations and re-parameterizations of a surface f . The corresponding set in SRNF representation is given by $[q] = \{O(q, \gamma) | O \in SO(3), \gamma \in \Gamma\}$. Each such class represents a shape uniquely and shapes are compared by computing a distance between the corresponding orbits. Similar to curves, the joint registration and shape comparison of surfaces is performed according to:

$$\inf_{\gamma \in \Gamma, O \in SO(3)} \|q_1 - O(q_2, \gamma)\| = \inf_{\gamma \in \Gamma, O \in SO(3)} \|O(q_1, \gamma) - q_2\| \quad . \quad (1.5)$$

While the optimization over $SO(3)$ is relatively straightforward, the optimization over Γ is much more difficult here than the curve case. We have developed a gradient-based approach that uses the geometry of the tangent space $T_{\gamma_{id}}(\Gamma)$. It uses a set of vector fields that incrementally deform the current grid on f_2 , so as to minimize the cost function given in Eqn. 1.5.

Similar to the case of constrained curves, the task of computing geodesics between any two registered surfaces is not trivial and requires a path straightening-algorithm (see Kurtek

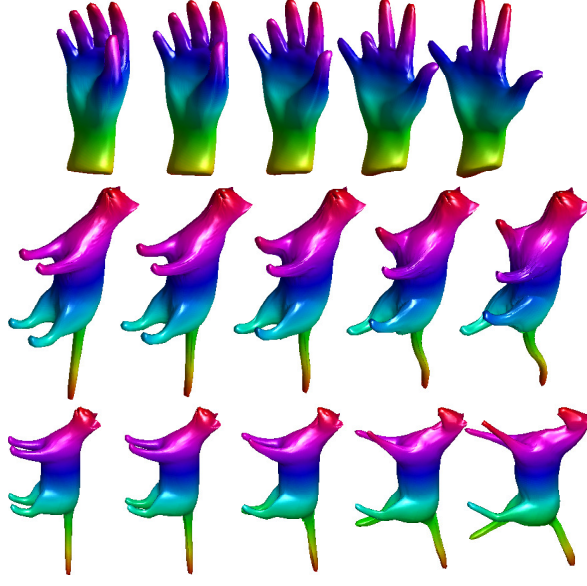


Figure 1.9 Each row shows an example of geodesic between a pair of objects (the starting and ending shapes).

et al. (2012a)). More recently, Xie et al. (2014a) have developed an approximation that first computes a straight-line geodesic between any two registered surfaces in the SRNF representation space, and then inverts each point along this geodesic to obtain a geodesic in the surface space. For more details, we refer the reader to these papers.

In Fig. 1.9, we show some examples of geodesics between objects including human hands and animals. In Fig. 1.10, we compare the geodesics between surfaces to the linear interpolation of surfaces. From the results, we can see that the tail part of the cat is distorted and inflated on the linearly interpolated path, but the tail part is better persevered along the geodesic path.

Using geodesics we can define and compute the mean shape using a standard algorithm for computing Karcher mean. Furthermore, we can define and compute Karcher covariance, and perform PCA on the tangent space at the mean shape. Figure 1.11 displays the observations and the k -th principal directions (PD) by constructing principal geodesics $\exp_{\mu}(ts_k \cdot \text{PC}_k)$, where $\text{PC}_k \in T_{\mu}(\mathcal{F})$ is the k^{th} principal component and s_k denotes the corresponding standard deviation. The PDs are displayed using the triples $\{\exp_{\mu}(-s_k \cdot \text{PC}_k), \mu, \exp_{\mu}(s_k \cdot \text{PC}_k)\}$. This analysis can be used to define a multivariate normal distribution on the principal coefficients and thus a random tangent vector from this Gaussian model. Assume that v is a random deformation of the mean surface, i.e., $v \in T_{\mu}(\mathcal{F})$ according to the normal model. Then, we can use the shooting method to get a random sample of surfaces such that $f = \exp_{\mu}(v)$. Several randomly sampled chess pieces are shown in Figure 1.11 bottom row.

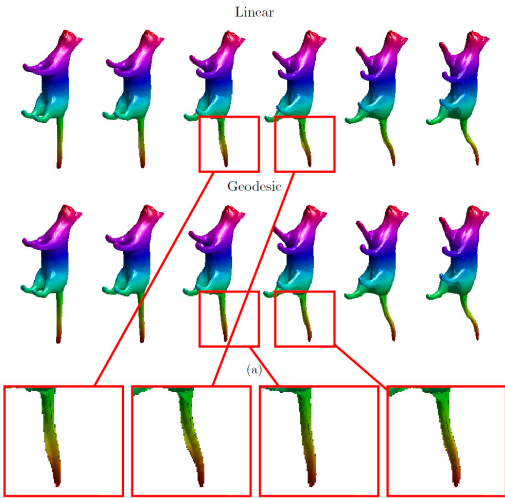


Figure 1.10 Comparing geodesic to linear interpolation.

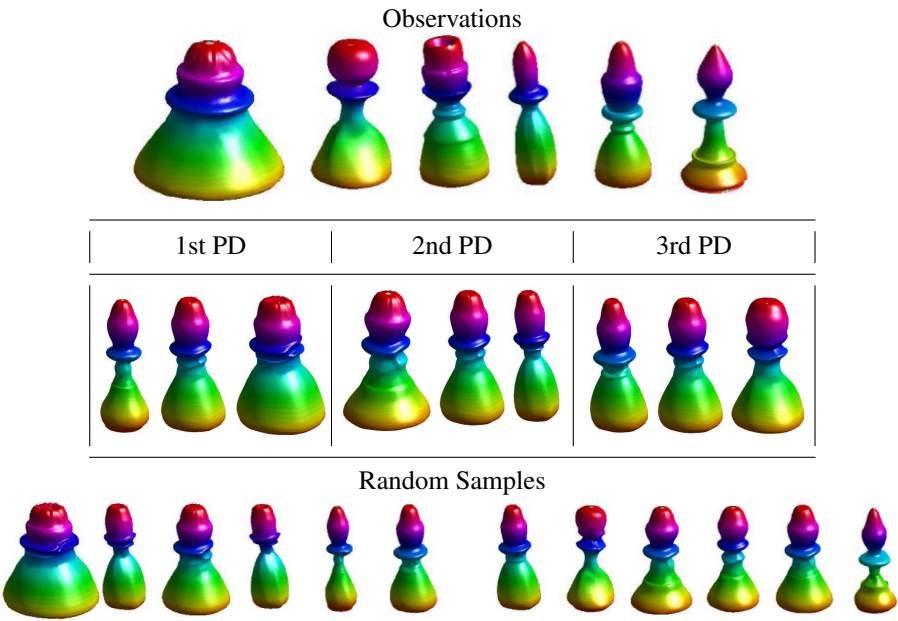


Figure 1.11 Computing mean shape, PC analysis and random samples under a Gaussian model. The first row shows some observations of chess piece. The second row shows the three main principal components. And the last row shows several randomly sampled chess pieces using a Gaussian model.

1.5 Metric-Based Image Registration

In the problem of image understanding, especially in object recognition and classification using image data, it is important to perform registration of images during their analysis. The importance of image registration comes across clearly in many applications. For example, in developing image templates of different letters and numbers in human handwriting, for the purposes of automated handwriting recognition, it is important to align images of same objects before averaging. To improve performance, it is often necessary to perform a nonrigid alignment, i.e. deform one image so as to match its pixel patterns with the other image as much as possible. While these deformations have been performed using various energy minimization methods in the past (Beg et al. 2005; Bookstein 1989; Collignon et al. 1997; Davies et al. 2002; Dupuis and Grenander 1998; Eriksson and Astrom 2006; Joshi et al. 2004; Lorenzen et al. 2005; Miller et al. 2002; Szeliski and Coughlan 1997; Thirion 1998; Troune 1998; Twining et al. 2004; Vercauteren et al. 2009; Viola and Wells III 1995), a novel idea is to use a proper metric for registration. As described in this section, there are several distinct advantages in this approach over the conventional ideas.

An image is treated as a function $f : D \rightarrow \mathbb{R}^n$, and the image space is $\mathcal{F} = \{f : D \rightarrow \mathbb{R}^n \mid f \in C^\infty(D)\}$. For a gray level image, we have $n = 1$, and for a colored image, we have $n = 3$. The domain of interest is $D = [0, 1]^2$, and the \mathbb{L}^2 metric is given by $\langle f_1, f_2 \rangle = \int_D \langle f_1(s), f_2(s) \rangle ds$. Let $\Gamma = \text{Diff}^+(D)$ be a subgroup of Diff^+ (the orientation-preserving diffeomorphism group) that preserves the boundary of D . A registration of image f_1 to image f_2 is to find a diffeomorphism $\gamma \in \Gamma$ such that pixel values $f_1(s)$ and $f_2(\gamma(s))$ are optimally matched to each other.

In the elastic framework, the mathematical representation of any image is given by a square-root map (SRM): $q(s) = \sqrt{a(s)}f(s)$, where $a(s)$ is the “generalized area multiplication factor” of f at $s \in D$. It takes the form $a(s) = |\mathbf{J}f(s)|_V$ where $|\mathbf{J}f(s)|_V = \left\| \frac{\partial f}{\partial x^1} \wedge \frac{\partial f}{\partial x^2} \right\|$. Here \wedge denotes the wedge product, $(x^1, x^2) : D \rightarrow \mathbb{R}^2$ are the coordinates on (a chart of) D and $\mathbf{J}f(s)$ is the Jacobian matrix of f at s with the (j, i) -th element as $\partial f^j / \partial x^i(s)$. The two special cases are: if $n = 2$, then $a(s) = |\mathbf{J}f(s)|$; if and $n = 3$, then $a(s) = \left\| \frac{\partial f}{\partial x^1}(s) \times \frac{\partial f}{\partial x^2}(s) \right\|$. Note that this SRM by definition applies to images such that $n \geq 2$. In case of gray level images, one can use their gradient images, $(f_u, f_v)(s) \in \mathbb{R}^2$, to fit into this representation. Intuitively, the SRM leaves uniform regions as zeros while preserving edge information in such a way that it is compatible with change of variables, i.e., stronger edges get higher values.

For $f \in \mathcal{F}$ and any γ , the SRM representation of $f \circ \gamma$ is given by $(q, \gamma) = \sqrt{|\mathbf{J}\gamma|}(q \circ \gamma)$. As mentioned earlier, under this representation, we have $\|q\| = \|(q, \gamma)\|$ and $\|(q_1, \gamma) - (q_2, \gamma)\| = \|q_1 - q_2\|$, for all q, q_1, q_2 and for all $\gamma \in \Gamma$. For the purpose of registration, we define an objective function between two images f_1 and f_2 by $\mathcal{L}(f_1, (f_2, \gamma)) = \|q_1 - (q_2, \gamma)\|$. The registration of two images is then achieved by minimizing the objective function according to:

$$\gamma^* = \underset{\gamma \in \Gamma}{\operatorname{arginf}} \mathcal{L}(f_1, (f_2, \gamma)) = \underset{\gamma \in \Gamma}{\operatorname{arginf}} \|q_1 - (q_2, \gamma)\|, \quad (1.6)$$

The optimization problem over Γ in Eqn. 1.6 forms the crux of our registration framework and is solved using a **gradient descent** method as in Kurtek et al. (2010); Xie et al. (2012, 2014b).

This registration framework satisfies a list fundamental properties such as: (1) it is invariant to simultaneous warping; (2) it is inverse consistent (Xie et al. 2014b). Additionally, the optimal registration is not affected by scaling and translations of image pixels: let $g_1 = c_1 f_1 + d_1$ and $g_2 = c_2 f_2 + d_2$ with $c_1, c_2 \geq 0$ and $d_1, d_2 \in \mathbb{R}^n$, if $\gamma^* = \arg \inf_{\gamma} \mathcal{L}(f_1, (f_2, \gamma))$ then $\gamma^* = \arg \inf_{\gamma} \mathcal{L}(g_1, (g_2, \gamma))$ as well.

In Fig. 1.12, we first present some results on synthetic images to demonstrate the use of the registration framework suggested in Eqn. 1.6. The images f_1 and f_2 are registered twice by first taking f_1 as the template image and estimating γ_{21} that optimally deforms f_2 using Eqn. 1.6. Then, the roles are reversed and f_2 is used as the template to obtain γ_{12} . We show the two converged energies, $\|(q_1, \gamma_{12}) - q_2\|$ and $\|q_1 - (q_2, \gamma_{21})\|$, associated with the optimal γ_{12} and γ_{21} to verify symmetry. The cumulative diffeomorphisms $\gamma_{21} \circ \gamma_{12}$ and $\gamma_{12} \circ \gamma_{21}$ are also used to demonstrate the inverse consistency of the proposed metric. The theory indicates that γ_{12} and γ_{21} are expected to be inverses of each other. We show the original images f_1 and f_2 with the matching warped images $f_2 \circ \gamma_{21}$ and $f_1 \circ \gamma_{12}$ respectively. The diffeomorphisms γ_{12} and γ_{21} learnt to register the images are also presented. By composing them in different orders we expect the resulting diffeomorphisms to be the identity map. In order to better visualize that the composed diffeomorphisms are close to identity, we apply them to checkerboard images. We observe that the composed diffeomorphisms $\gamma_{21} \circ \gamma_{12}$ and $\gamma_{12} \circ \gamma_{21}$ are close to the identity map.

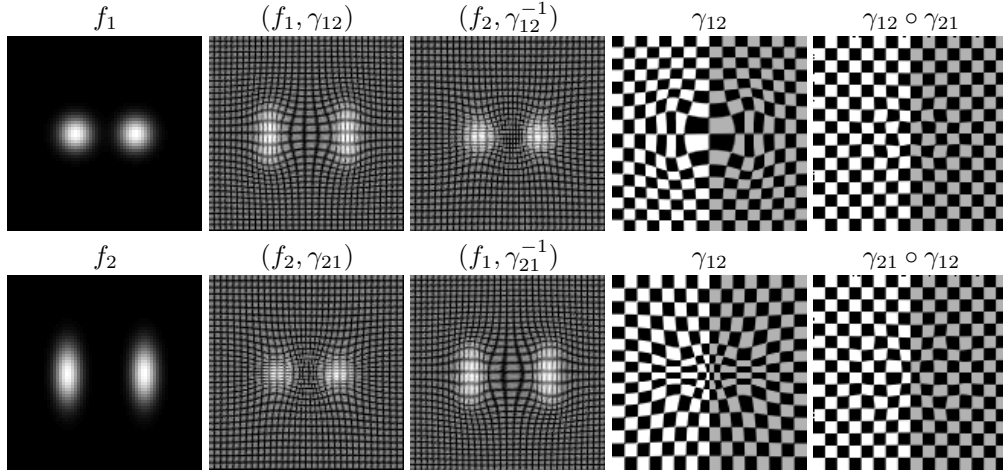


Figure 1.12 Registering Synthetic Smooth Grayscale Images. $\gamma_{12} = \arg \inf_{\gamma \in \Gamma} \|(q_1, \gamma) - q_2\|$ and $\gamma_{21} = \arg \inf_{\gamma \in \Gamma} \|q_1 - (q_2, \gamma)\|$. $\|q_1 - q_2\| = 0.2312$, $\|q_1 - (q_2, \gamma_{21})\| = 0.0728$ and $\|(q_1, \gamma_{12}) - q_2\| = 0.0859$.

In Fig. 1.13, we present registration results using 2D brain MR images. In order to illustrate our method, in each of the two experiments, we show (1) the original images overlapped f_1/f_2 and (2) overlapped images after registration ($f_1/f_2 \circ \gamma_{21}$ and $f_2/f_1 \circ \gamma_{12}$). The overlapped images show image pairs in a common canvas.

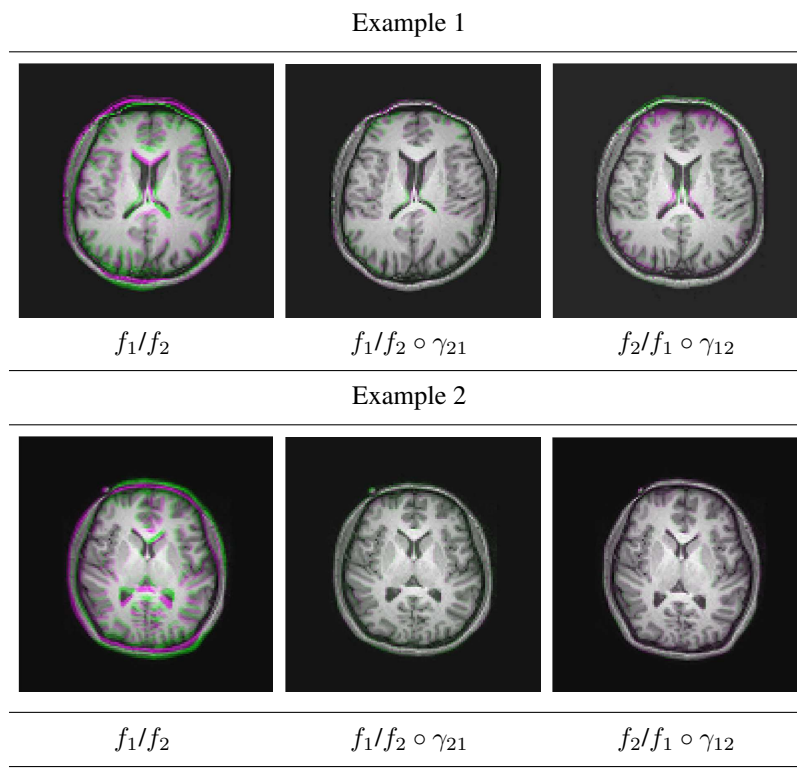


Figure 1.13 Two examples of brain MR image registration (each row as an example). First column shows overlapped original images f_1 and f_2 ; second column shows overlapped images f_1 and deformed f_2 ; third column shows f_2 and deformed f_1 .

When objects in images have some specific landmarks, either provided by experts or some additional data analysis, they can provide some guidance in defining image correspondence. Automated registration methods routinely produce results that conflict with our contextual knowledge, and annotated landmarks provide a way to reconcile these two ideas. The framework can be further extended so that landmark information is incorporated during registration and all of the nice mathematical properties of the objective function are preserved.

Two pairs of 2D brain MR images are used to illustrate this procedure. In Fig. 1.14, we want to register f_1 to f_2 . Four landmark points are provided and are displayed in each image as yellow dots. The images are first registered using only the landmarks, with a kernel based approach, and the resulting deformed image is f_1^{lm} . We further deform f_1^{lm} by applying our registration method as in Eqn. 1.6 with restricted vector fields, specified by a set of basis so that the landmark points remain intact. The final result is shown as (f_1^{lm}, γ) and are compared to registration without landmarks as f_1^{lm} . The optimally deformed f_1 without landmark information is displayed in the last column as (f_1, γ) as a baseline. Since the deformation in the skull is so large that our method gives a local solution. By adopting the landmark-aided

registration, we at first get a deformed image f_1^{lm} , with the landmarks nicely matched and the skull deformed correspondingly. Then f_1^{lm} is further deformed to register the intensity details without moving the landmarks. The final result (f_1^{lm}, γ) matches f_2 with no artifacts around the skull. Generally, the registration with landmarks outperforms registration without landmarks.

1.6 Summary and Future Work

We have presented an overview of elastic shape analysis for several kinds of objects, including Euclidean curves, surfaces in \mathbb{R}^3 , real-valued functions on $[0, 1]$, and 2D images. The analysis is characterized by a simultaneous registration of points across objects and comparisons of their shapes. The key idea is to restrict to parameterized objects and to use parameterization as a tool for registration under metrics that are invariant to all shape-preserving transformations, including re-parameterizations. The use of such metrics is facilitated by square-root mappings of original data because under these mappings, the original metrics become the standard \mathbb{L}^2 metric. For each of the data type considered, we present the corresponding square-root transformation and demonstrate some associated statistical tools.

In terms of future work, there are several questions associated with this framework that remain open. An important issue in choosing the elastic metric (or the related square-root representation) is the uniqueness. For instance, in the context of FDA and phase-amplitude separation, one can pose the question: Are there other transforms that allow, under the \mathbb{L}^2 metric, an appropriate framework for function registration? In fact, there exist other mappings, e.g. $f(t) \mapsto G(f(t), \dot{f}(t))\sqrt{|\dot{f}(t)|}$, where G is an arbitrary function of f and \dot{f} , that leads to isometry under the \mathbb{L}^2 norm. However, their pros and cons in different situations needs to be explored further.

Another important area in shape analysis of curves is the groups beyond the similarity transformations. We have already mentioned the paper by Bryner et al. (2014) that provides affine-invariant shape analysis of elastic curves. However, such an elastic analysis of planar curves that is invariant under projective transformation group, remains to be developed.

References

- Bauer M, Bruveris M and Michor PW 2013 R-transforms for Sobolev H^2 -metrics on spaces of plane curves. *eprint arXiv:1311.3526*.
- Beg M, Miller M, Trounev A and Younes L 2005 Computing large deformation metric mappings via geodesic flows of diffeomorphisms. *International Journal of Computer Vision* **61**, 139–157.
- Bookstein FL 1989 Principal warps: Thin-plate splines and the decomposition of deformations. *IEEE Transactions on Pattern Analysis and Machine Intelligence* **11**(6), 567–585.
- Bryner D, Klassen E, Le H and Srivastava A 2014 2D affine and projective shape analysis. *Pattern Analysis and Machine Intelligence, IEEE Transactions on* **36**(5), 998–1011.
- Collignon A, Vandermeulen D, Marchal G and Suetens P 1997 Multimodality image registration by maximization of mutual information. *IEEE Transactions on Medical Imaging* **16**(2), 187–198.
- Davies R, Twining C, Cootes T, Waterton J and Taylor C 2002 A minimum description length approach to statistical shape modeling. *IEEE Transactions on Medical Imaging* **21**(5), 525–537.
- Dryden I and Mardia K 1998 *Statistical Shape Analysis* Wiley series in probability and statistics. Wiley.
- Dupuis P and Grenander U 1998 Variational problems on flows of diffeomorphisms for image matching. *Journal Quarterly of Applied Mathematics* **LVI**(3), 587–600.
- Eriksson A and Astrom K 2006 Bijective image registration using thin-plate splines. *Pattern Recognition, International Conference on*, vol. 3, pp. 798–801.

- Grenander U and Miller MI 1998 Computational anatomy: An emerging discipline. *Quarterly of Applied Mathematics* **LVI**(4), 617–694.
- Jeannin S and Bober M 1999 Shape data for the MPEG-7 core experiment ce-shape-1 @ONLINE.
- Jermyn IH, Kurtek S, Klassen E and Srivastava A 2012 Elastic shape matching of parameterized surfaces using square root normal fields *Proceedings of the 12th European Conference on Computer Vision - Volume Part V*, pp. 804–817, Berlin, Heidelberg.
- Joshi S, Davis B, Jomier BM and B GG 2004 Unbiased diffeomorphic atlas construction for computational anatomy. *Neuroimage* **23**, 151–160.
- Karcher H 1977 Riemannian center of mass and mollifier smoothing. *Communications on Pure and Applied Mathematics* **30**(5), 509–541.
- Kent JT and Mardia KV 2012 A geometric approach to projective shape and the cross ratio. *Biometrika* **99**(4), 833–849.
- Kneip A and Ramsay JO 2008 Combining registration and fitting for functional models. *Journal of the American Statistical Association*.
- Kurtek S, Klassen E, Ding Z and Srivastava A 2010 A novel Riemannian framework for shape analysis of 3D objects *Computer Vision and Pattern Recognition (CVPR), 2010 IEEE Conference on*, pp. 1625–1632.
- Kurtek S, Klassen E, Ding Z, Jacobson SW, Jacobson JB, Avison M and Srivastava A 2011 Parameterization-invariant shape comparisons of anatomical surfaces. *IEEE Transactions on Medical Imaging* **30**(3), 849–858.
- Kurtek S, Klassen E, Gore JC, Ding Z and Srivastava A 2012a Elastic geodesic paths in shape space of parameterized surfaces. *IEEE Transactions on Pattern Analysis and Machine Intelligence* **34**(9), 1717–1730.
- Kurtek S, Srivastava A, Klassen E and Ding Z 2012b Statistical modeling of curves using shapes and related features. *Journal of the American Statistical Association* **107**(499), 1152–1165.
- Liu W, Srivastava A and Zhang J 2010 Protein structure alignment using elastic shape analysis *Proceedings of the First ACM International Conference on Bioinformatics and Computational Biology*, pp. 62–70 BCB '10. ACM, New York, NY, USA.
- Liu W, Srivastava A and Zhang J 2011 A mathematical framework for protein structure comparison. *PLOS Computational Biology*.
- Lorenzen P, Davis B and Joshi S 2005 Unbiased atlas formation via large deformations metric mapping In *Medical Image Computing and Computer-Assisted Intervention MICCAI 2005* (ed. Duncan J and Gerig G) vol. 3750 of *Lecture Notes in Computer Science* Springer Berlin Heidelberg pp. 411–418.
- Mardia KV and Dryden IL 1989 The statistical analysis of shape data. *Biometrika* **76**(2), pp. 271–281.
- Miller M, Trounev A and Younes L 2002 On the metrics and Euler-Lagrange equations of computational anatomy. *Annual Review of Biomedical Engineering* **4**, 375–405.
- Ramsay JO and Li X 1998 Curve registration. *Journal of the Royal Statistical Society: Series B (Statistical Methodology)* **60**(2), 351–363.
- Ramsay JO and Silverman BW 2005 *Functional Data Analysis* Springer Series in Statistics 2nd edn. Springer.
- Samir C, Kurtek S, Srivastava A and Canis M 2014 Elastic shape analysis of cylindrical surfaces for 3D/2D registration in endometrial tissue characterization. *Medical Imaging, IEEE Transactions on* **33**(5), 1035–1043.
- Srivastava A, Joshi SH, Mio W and Liu X 2005 Statistical shape analysis: Clustering, learning, and testing. *IEEE Transactions on Pattern Analysis and Machine Intelligence* **27**(4), 590–602.
- Srivastava A, Klassen E, Joshi SH and Jermyn IH 2011a Shape analysis of elastic curves in Euclidean spaces. *IEEE Transactions on Pattern Analysis and Machine Intelligence* **33**(7), 1415–1428.
- Srivastava A, Wu W, Kurtek S, Klassen E and Marron JS 2011b Registration of functional data using Fisher-Rao metric. *arXiv:1103.3817v2*.
- Su J, Kurtek S, Klassen E and Srivastava A 2014 Statistical analysis of trajectories on Riemannian manifolds: Bird migration, hurricane tracking and video surveillance. *The Annals of Applied Statistics* **8**(1), 530–552.
- Szeliski R and Coughlan J 1997 Spline-based image registration. *International Journal of Computer Vision* **22**(3), 199–218.
- Tang R and Muller HG 2008 Pairwise curve synchronization for functional data. *Biometrika* **95**(4), 875–889.
- Thirion J 1998 Image matching as a diffusion process: an analogy with Maxwell's demons. *Medical Image Analysis* **2**(3), 243–260.
- Trounev A 1998 Diffeomorphisms groups and pattern matching in image analysis. *International Journal of Computer Vision* **28**(3), 213–221.
- Tucker J, Wu W and Srivastava A 2012 Analysis of signals under compositional noise with applications to sonar data *Oceans, 2012*, pp. 1–6.
- Tucker JD, Wu W and Srivastava A 2013 Generative models for functional data using phase and amplitude separation. *Comput. Stat. Data Anal.* **61**, 50–66.
- Twining C, Marsland S and Taylor C 2004 Groupwise non-rigid registration: The minimum description length approach. *Proceedings of the British Machine Vision Conference (BMVC)* **1**, 417–426.
- Vercauteren T, Pennec X, Perchant A and Ayache N 2009 Diffeomorphic demons: Efficient non-parametric image registration. *NeuroImage* **45**(Supplement 1), S61–S72.

- Viola P and Wells III W 1995 Alignment by maximization of mutual information *Computer Vision, Fifth International Conference on*, pp. 16–23.
- Xie Q, Jermyn I, Kurtek S and Srivastava A 2014a Numerical inversion of SRNFs for efficient elastic shape analysis of star-shaped objects *European Conference on Computer Vision (ECCV)*.
- Xie Q, Kurtek S, Christensen GE, Ding Z, Klassen E and Srivastava A 2012 A novel framework for metric-based image registration *Proceedings of the 5th International Conference on Biomedical Image Registration*, pp. 276–285 WBIR'12. Springer-Verlag, Berlin, Heidelberg.
- Xie Q, Kurtek S, Klassen E, Christensen GE and Srivastava A 2014b Metric-based pairwise and multiple image registration *2014 European Conference on Computer Vision (ECCV)*.
- Xie Q, Kurtek S, Le H and Srivastava A 2013 Parallel transport of deformations in shape space of elastic surfaces *2013 IEEE International Conference on Computer Vision (ICCV)*, pp. 865–872.

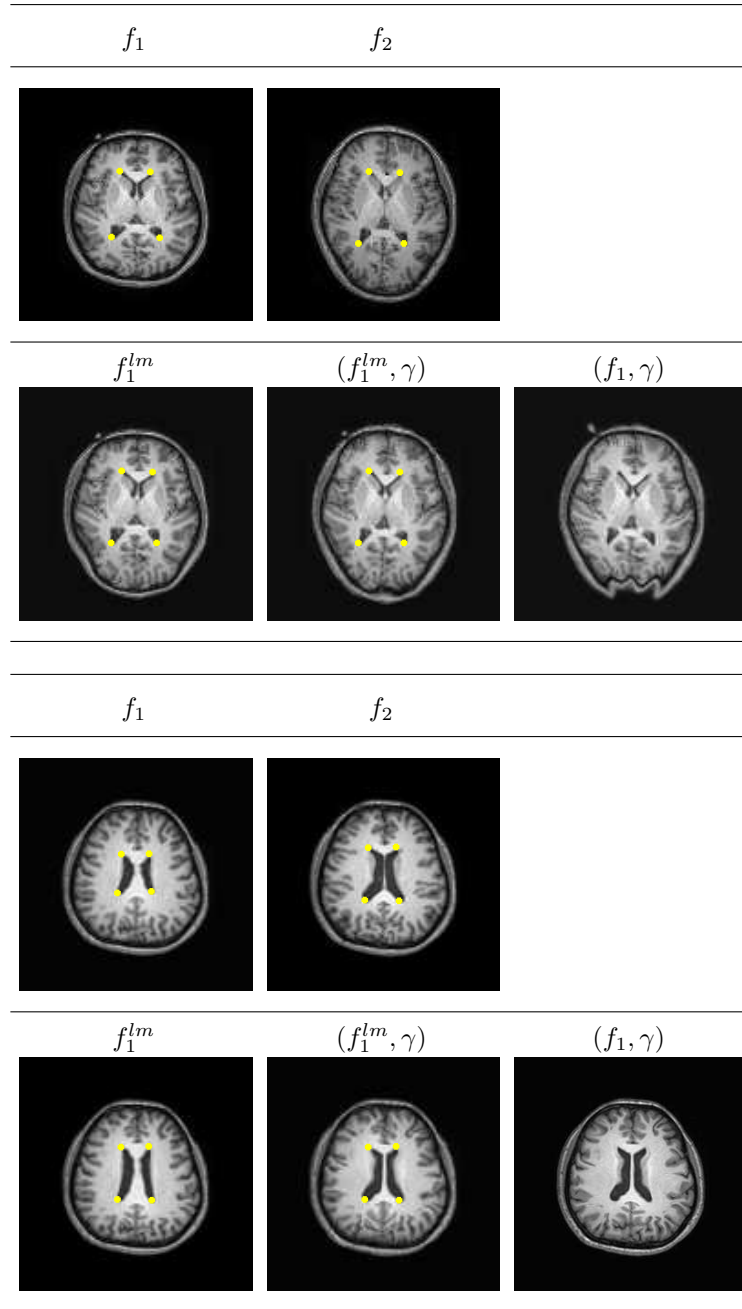


Figure 1.14 Two examples of brain image registration with landmarks. In each experiment, the top row shows the original images f_1 and f_2 , and in the bottom row, the first column shows the deformed images f_1^{lm} using only landmarks; the second column shows the final deformed images (f_1^{lm}, γ) with f_1^{lm} as the initial condition; and the last column shows the registered images (f_1, γ) without involving landmarks.